Heliyon 9 (2023) e18454

Contents lists available at ScienceDirect

Heliyon

journal homepage: www.cell.com/heliyon

Study on the calibration of full polarization imager

Tianquan Liang [a,*], Qingxin Tang [a], Quanzhou Yu [a]

[a] School of Geography and Environment, Liaocheng University, Liaocheng 252059, PR China

ARTICLE INFO

Keywords:
Polarization
Radiometric calibration
Polarization calibration
Full Stokes vectors

ABSTRACT

Polarization is one of the fundamental properties of light, which has a wide range of applications and is developing rapidly. To meet the needs of polarization detection, different types of polarization instruments came into being. The precision of the polarization detection instruments is vital to the result analysis. In this paper, a full polarization imager is designed, and the radiometric calibration and polarization calibration of this instrument are studied. In radiometric calibration, the different numbers lights are set to verify the light intensity response of the imager. The mathematical model was constructed for numerical fitting, and the correlation between the fitted values and the measured values in the 490 nm, 550 nm, and 670 nm bands was above 0.99. Fixed the radiance of the integrating sphere, and adjusted exposure times. The correlation of the three bands is above 0.99, which verifies that the radiative stability of the imager is good. The polarimetric calibration system adopts the adjustable degree of polarization reference light source (APOL). The theoretical and measured values of the degree of polarization of reference light sources in three different bands are analyzed. The results show that the measurement accuracy of the 490 nm band is less than 2%. The precision of polarization measurement in the 550 nm band is less than 1.5%, and the precision of polarization calibration in the 670 nm band is less than 1%. The imager is verified to have high polarization calibration accuracy and meets the requirements of high-precision polarization detection.

1. Introduction

Polarization of light has been widely used in many fields since it was discovered by Rasmus Bartholin in 1669. Polarization, intensity, phase, and spectrum together constitute the fundamental properties of light. Among them, research on polarization characteristics is gradually receiving attention [1–3]. Polarization is widely used in deep space planetary exploration, target detection and characterization, aerosol microphysical characteristics analysis, atmospheric correction, vegetation ecology, biomedical, bionic navigation, and other fields [4–9].

To effectively interpret the polarization characteristics of light, different types of instruments are designed to obtain polarized light information [10–14]. The polarization instruments can be divided into ground polarization instruments, airborne polarimetric instruments, and aerospace polarization instruments according to application requirements. According to different working modes, it can be divided into time division polarization imager and simultaneous polarization imager. Especially in recent years, satellite polarimetric remote sensing has developed rapidly. Such as POLDER (Polarization and Directionality of the Earth's Reflectance instrument) sensor, GOME (Global Ozone Monitoring Experiment) sensor, SCIAMACHY (SCanning Imaging Absorption spectroMeter for

* Corresponding author.
E-mail address: liangpolaris@126.com (T. Liang).

https://doi.org/10.1016/j.heliyon.2023.e18454
Received 9 July 2023; Received in revised form 18 July 2023; Accepted 18 July 2023
Available online 19 July 2023

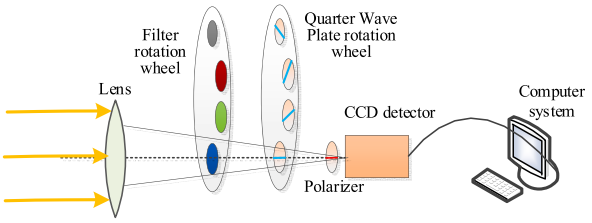

Fig. 1. Schematic diagram of the full polarization imager structure.

Atmospheric CHartographY) sensor, MAP (Multi-Angle Polarimeter) sensor, APS (Aerosol Polarimetry Sensor) sensor, HARP (Hyper-Angular Rainbow Polarimeter) sensor, CALIOP (Cloud-Aerosol LIdar with Orthogonal Polarization) sensor, MAIA (Multi-Angle Imager for Aerosols) sensor, CAPI (Cloud and Aerosol Polarization Imager) sensor, MAI (Multi-Angle polarization Imager) sensor, DPC (Directional Polarimetric Camera) sensor, POSP (Particulate Observing Scanning Polarimeter) sensor, PCF (Polarization CrossFire Suite) sensor, SGLI (Second Generation Global Imager) sensor, and MISR (Multiangle Imaging SpectroRadiometer) sensor, etc [15–22]. The application of commercial polarization CCD (Charge-Coupled Device) has also made significant progress.

To ensure the accuracy of measurement data, the instrument needs a standard source to calibrate [23–25]. In this paper, the calibration method of a full polarization imager is studied, which mainly includes two aspects: radiation calibration and polarization calibration. Radiometric calibration of polarization imager determines the quantitative relationship between the input radiation quantity (quantity with radiance value dimension) and the output radiation quantity of each band of the imager. Polarization calibration of the polarization imager refers to the quantitative relationship between the standard polarization reference source, which can theoretically trace the polarization characteristics and the output value of the polarization imager [26–28].

In this paper, radiation calibration and polarization calibration of a full polarization imager are studied, and the feasibility of the calibration process is verified. The results can quantitatively evaluate the performance of the polarization imager and ensure the accuracy and stability of the polarization imager data. The corresponding calibration process can provide robust technical support for the performance verification of other polarization imaging instruments.

2. Experimental instrument

To effectively characterize the polarization characteristics of light, a full polarization imager is designed, which can retrieve full Stokes vectors. By interpreting the full Stokes vector of the detection light wave, the target information detected by the imager can be characterized more effectively.

As shown in Fig. 1, the full polarization imager adopts the modulation mode of a combination of quarter wave plate and polarizer. The polarizer is GPM-100-UNC produced by Meadowlark Company, with an effective wavelength range of 300–2700 nm for extinction coefficient response. It has an extremely broadband polarizer solution with up to 1,000,000:1 contrast ratio. The working way is fixed polarizer and rotating wave plate, and the light transmission axis of the polarizer coincides with the reference 0° fast axis direction determined by the wave plate. The Muller matrix of a phase retarder with an azimuth of γ and a delay of Δ is expressed in the following formula (1).

$$M_b = \begin{bmatrix} 1 & 0 & 0 & 0 \\ 0 & 1-(1-\cos\Delta)\sin^2 2\gamma & (1-\cos\Delta)\sin 2\gamma\cos 2\gamma & -\sin\Delta\sin 2\gamma \\ 0 & (1-\cos\Delta)\sin 2\gamma\cos 2\gamma & 1-(1-\cos\Delta)\cos^2 2\gamma & \sin\Delta\cos 2\gamma \\ 0 & \sin\Delta\sin 2\gamma & -\sin\Delta\cos 2\gamma & \cos\Delta \end{bmatrix} \tag{1}$$

For a phase retarder with azimuth γ and delay of a quarter wavelength, the following formula (2) expression can be obtained.

$$M_b = \begin{bmatrix} 1 & 0 & 0 & 0 \\ 0 & \cos^2 2\gamma & \sin 2\gamma\cos 2\gamma & -\sin 2\gamma \\ 0 & \sin 2\gamma\cos 2\gamma & \sin^2 2\gamma & \cos 2\gamma \\ 0 & \sin 2\gamma & -\cos 2\gamma & 0 \end{bmatrix} \tag{2}$$

The Muller matrix of a polarizer with an azimuth of θ can be expressed as formula (3).

$$M_P = \frac{1}{2}\begin{bmatrix} P_1^2+P_2^2 & (P_1^2-P_2^2)\cos 2\theta & (P_1^2-P_2^2)\sin 2\theta & 0 \\ (P_1^2-P_2^2)\cos 2\theta & (P_1^2+P_2^2)\cos^2 2\theta + 2P_1P_2\sin^2 2\theta & (P_1^2-P_2^2)\sin 2\theta\cos 2\theta & 0 \\ (P_1^2-P_2^2)\sin 2\theta & (P_1-P_2)^2\sin 2\theta\cos 2\theta & (P_1^2+P_2^2)\sin^2 2\theta + 2P_1P_2\cos^2 2\theta & 0 \\ 0 & 0 & 0 & 2P_1P_2 \end{bmatrix} \tag{3}$$

When $P_1 = 1$ and $P_2 = 0$ in equation (3), it indicates that the polarizer is a fully linear polarizer, and its Muller matrix can be represented as formula (4).

Table 1
Uncertainty source of integrating sphere calibration light source calibration.

Wavelength (nm)	450–800	800–1000	1000–2000	2000–2500
Synthetic uncertainty of radiometer calibration	2.60–1.81	1.86–2.91	1.59–4.06	1.63–3.78
Angular uniformity	0.6 (Maximum within ±4°)			
Surface uniformity	0.48			
stability	0.09			
The total uncertainty of result synthesis	2.71–1.97	2.01–3.01	1.77–4.13	1.80–3.86

The calibration light source of the integrating sphere measures the standard lamp-reference plate system by the HR1024 spectral radiometer of the SVC company, and then transmits the monochromatic radiance dimension of the emitted light with different radiation levels to the integrating sphere. The sources of measurement uncertainty of the spectral radiometer are shown in Table 2

$$M_p = \frac{1}{2}\begin{bmatrix} 1 & \cos 2\theta & sin2\theta & 0 \\ \cos 2\theta & \cos^2 2\theta & sin2\theta \cos 2\theta & 0 \\ sin2\theta & sin2\theta \cos 2\theta & sin^2 2\theta & 0 \\ 0 & 0 & 0 & 0 \end{bmatrix} \tag{4}$$

The complete optical wave polarization state transfer link of the full polarization imager can be expressed as formula (5).

$$\begin{bmatrix} I_0 \\ Q_0 \\ U_0 \\ V_0 \end{bmatrix} = M_p M_b S_{in} = \frac{1}{2}\begin{bmatrix} 1 & \cos 2\theta & sin2\theta & 0 \\ \cos 2\theta & \cos^2 2\theta & sin2\theta \cos 2\theta & 0 \\ sin2\theta & sin2\theta \cos 2\theta & sin^2 2\theta & 0 \\ 0 & 0 & 0 & 0 \end{bmatrix} * \begin{bmatrix} 1 & 0 & 0 & 0 \\ 0 & \cos^2 2\gamma & sin2\gamma \cos 2\gamma & -sin2\gamma \\ 0 & sin2\gamma \cos 2\gamma & sin^2 2\gamma & \cos 2\gamma \\ 0 & sin2\gamma & -\cos 2\gamma & 0 \end{bmatrix} * \begin{bmatrix} I_i \\ Q_i \\ U_i \\ V_i \end{bmatrix} \tag{5}$$

Formula (6) can be obtained by further arrangement.

$$\begin{bmatrix} I_0 \\ Q_0 \\ U_0 \\ V_0 \end{bmatrix} = M_p M_b S_{in} = \frac{1}{2}\begin{bmatrix} 1 & \cos 2\theta & sin2\theta & 0 \\ \cos 2\theta & \cos^2 2\theta & sin2\theta \cos 2\theta & 0 \\ sin2\theta & sin2\theta \cos 2\theta & sin^2 2\theta & 0 \\ 0 & 0 & 0 & 0 \end{bmatrix} * \begin{bmatrix} I_i \\ \cos^2 2\gamma * Q_i + sin2\gamma \cos 2\gamma * U_i - sin2\gamma * V_i \\ sin2\gamma \cos 2\gamma * Q_i + sin^2 2\gamma * U_i + \cos 2\gamma * V_i \\ sin2\gamma * Q_i - \cos 2\gamma * V_i \end{bmatrix} \tag{6}$$

The relationship between the radiation intensity detected by the full polarization imager and the Stokes vector of the incident light wave can be expressed as formula (7).

$$I_{(\theta,\gamma)} = \frac{1}{2}\left\{I_i + \cos 2\theta * \left[\cos^2 2\gamma * Q_i + sin2\gamma \cos 2\gamma * U_i - sin2\gamma * V_i\right] + sin2\theta * \left(sin2\gamma \cos 2\gamma * Q_i + sin^2 2\gamma * U_i + \cos 2\gamma * V_i\right)\right\} \tag{7}$$

The direction of the light transmission axis of the polarizer is fixed, so that θ = 0. Therefore, the angle variable in Equation (7) is reduced to one. The choice of quarter wave plate angle γ should take into account the sensitivity to different incident luminous fluxes and the error sensitivity caused by installation angle deviation, setting the γ angle of the quarter wave plate at (0°, 30°, 60°, −45°). The full Stokes vector is resolved as formula (8).

$$\begin{cases} I_i = \dfrac{2(2\sqrt{3}-3)}{3}\left[(-I_{0^0}) + 2(I_{30^0} + I_{60^0}) + 2\sqrt{3}I_{-45^0}\right] \\ Q_{\mathrm{i}} = 2I_{0^0} + \dfrac{2(3-2\sqrt{3})}{3}\left[(-I_{0^0}) + 2(I_{30^0} + I_{60^0}) + 2\sqrt{3}I_{-45^0}\right] \\ U_i = \dfrac{4\sqrt{3}}{3}(I_{30^0} - I_{60^0}) \\ V_{\mathrm{i}} = 2I_{-45^0} + \dfrac{2(3-2\sqrt{3})}{3}\left[(-I_{0^0}) + 2(I_{30^0} + I_{60^0}) + 2\sqrt{3}I_{-45^0}\right] \end{cases} \tag{8}$$

The mathematical definitions of the degree of polarization degree, the degree of linear polarization, and the degree of circular polarization of the full polarization imager are shown in formulas (9) ~ (11), respectively.

$$DoP = \frac{\sqrt{Q^2 + U^2 + V^2}}{I} \tag{9}$$

$$DoLP = \frac{\sqrt{Q^2 + U^2}}{I} \tag{10}$$

$$DoCP = \frac{\sqrt{V^2}}{I} \tag{11}$$

Table 2
Sources of uncertainty in measurement response of the spectral radiometer.

Wavelength (nm)	450–800	800–1000	1000–1800	1800–2500
Combined uncertainty of standard lamp-reference plate system	1.75–1.51	1.57–2.75	1.57–2.75	1.57–2.75
Radiometer wavelength deviation	0.5–0.06	0.06–0.2	0.14–0.32	0.4–0.59
Class A evaluation of measuring	0.49–0.07	0.07–0.52	0.04–0.02	0.04–0.05
Nonlinear	1.7–0.97	0.97–0.39	0.12–2.82	0.18–2.52
Instability	0.55–0.20	0.20–0.67	0.13–0.91	0.1–0.19
Synthetic uncertainty of spectral radiometer response	2.60–1.81	1.86–2.91	1.59–4.06	1.63–3.78

Table 3
Monochromatic radiance of the integrating sphere with different numbers of lights on and various wavebands.

Wavelength (nm)		490	550	670	870
number of lights on	1	0.34887	0.61321	1.14804	1.62246
	2	0.69306	1.2159	2.27072	3.21703
	4	1.47528	2.56109	4.70755	6.61632
	8	3.0389	5.24451	9.5509	13.4462
	16	5.70826	9.84118	17.836	25.2867
	24	9.08468	15.6545	28.3117	40.3792
	32	12.06407	20.8014	37.6794	53.5815

Table 4
S_0 component values of different wavelengths and varying lighting levels.

Wavelength (nm)		490	550	670
number of lights on	1	24006.6864	38440.497	26448.3295
	2	50907.2624	65344.9298	42244.1895
	4	94840.8334	123742.4403	75736.8931
	8	181767.788	239982.903	141462.4842
	16	327838.6835	435336.6097	253163.2521
	24	509394.6555	674697.1035	393684.2723
	32	671412.5623	818999.3693	518036.543

3. Results and discussion

3.1. Full polarization imager radiometric calibration

Radiometric calibration usually requires a stable calibration light source, and a self-developed 2.5 m diameter integrating sphere calibration light source is used. The origins of uncertainty in integrating sphere calibration light sources mainly include angle inhomogeneity, surface inhomogeneity, and stability. The specific values are shown in the following Table 1.

Through the above data analysis, it can be seen that the uncertainty of the measurement system is transferred and superimposed. The combined total uncertainty is the sum of the combined uncertainty of the standard lamp-reference plate system, the measurement response uncertainty of the spectral radiometer, and the uncertainty of integrating sphere calibration light source. Among them, the Class A evaluation refers to the assessment of various random factors. The temperature of the radiometric calibration environment is 22 °C and the humidity is 48%. For the use of the polarization imager, combined with the band, the values of different radiance levels of the integrating sphere of the corresponding band are given, as shown in the following table.

Among them, in Table 3, the unit of turning on the light is the lamp, the unit of wavelength is nm, and the dimension of the monochromatic radiance value is W/(cm^2·sr·nm). Different wavelengths of the polarization imager and different levels of turning on lights determined by the radiance dimension of the integrating sphere are tested, respectively.

For the experimental results of different bands, the S_0 component of the Stokes parameter, that is, the intensity component, and the corresponding values of varying lighting levels are calculated respectively, as shown in Table 4.

The Stokes S_0 component obtained by different wavelengths and various levels of lights on is calculated using the least square method. The measured data and the fitting results are shown in Fig. 2(a–c). The radiometric calibration scene is shown in Fig. 2(d).

The actual measured data of three different bands are numerically fitted using the following formula (12) mathematical model.

$$y = Ax + B \tag{12}$$

The mathematical model coefficients of three bands and the adjusted R-Squared, as shown in the following table.

As seen in Fig. 2 and Table 5, the correlation between the fitting value and the measured value of the radiance value of the integrating sphere at different levels of the 490 nm band is 0.99916. At the 550 nm band, the correlation between the fitting value and the measured value of the radiance value of the integrating sphere of different levels is 0.99533. The correlation between the fitting

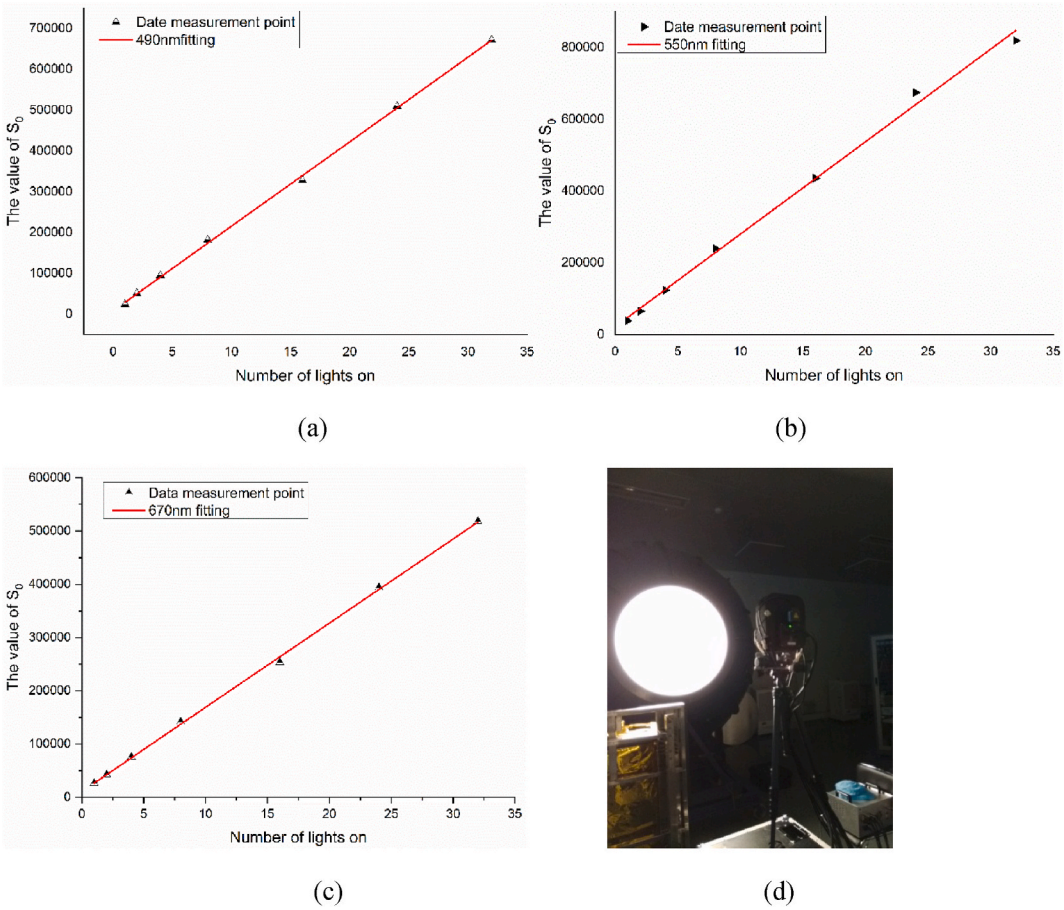

Fig. 2. (A)–(c) show the fitting results of different light-on levels in 490 nm, 550 nm and 670 nm bands, respectively, and (d) show the radiometric calibration scene.

Table 5
Model coefficients and Adjusted R-Squared values in different bands.

Wavelength (nm)	490	550	670
A	20700.1129	25781.17	15808.40941
B	8465.52107	21940.25	10777.76353
Adj. R-Square	0.99916	0.99533	0.99918

values of varying levels of the radiance of integrating sphere in the 670 nm band and the measured values is 0.99918. Through the analysis of the results, the radiation stability of the full polarization imager is good.

To thoroughly verify the stability of the imager, the number of lights on the integrating sphere is fixed, the exposure time of the camera is adjusted, and the data results are observed. The mathematical model expressed by formula (9) is used for the numerical fitting. The data results of the three bands are shown in Fig. 3(a–c). The model coefficients and Adjusted R-Squared values are shown in Table 6.

3.2. *Polarization calibration of the polarization imager*

The polarization calibration system adopts the adjustable degree of polarization reference light source (APOL), which has the characteristics of high accuracy and large dynamic range adjustment. The radiant light source is homogenized by integrating sphere and collimated by a beam expander to form a light source with high uniformity and parallelism. Polarized light with different degrees of polarization is generated by four flat glasses.

A beam of completely unpolarized light is incident on the flat glass at angle i, and the incident light is divided into reflected light and transmitted light. If the light beam is projected and output through flat glass after multiple refractions, the outgoing light wave is the superposition of all projected light beams. When the light source irradiates the polarization generator at incident angle i, the degree

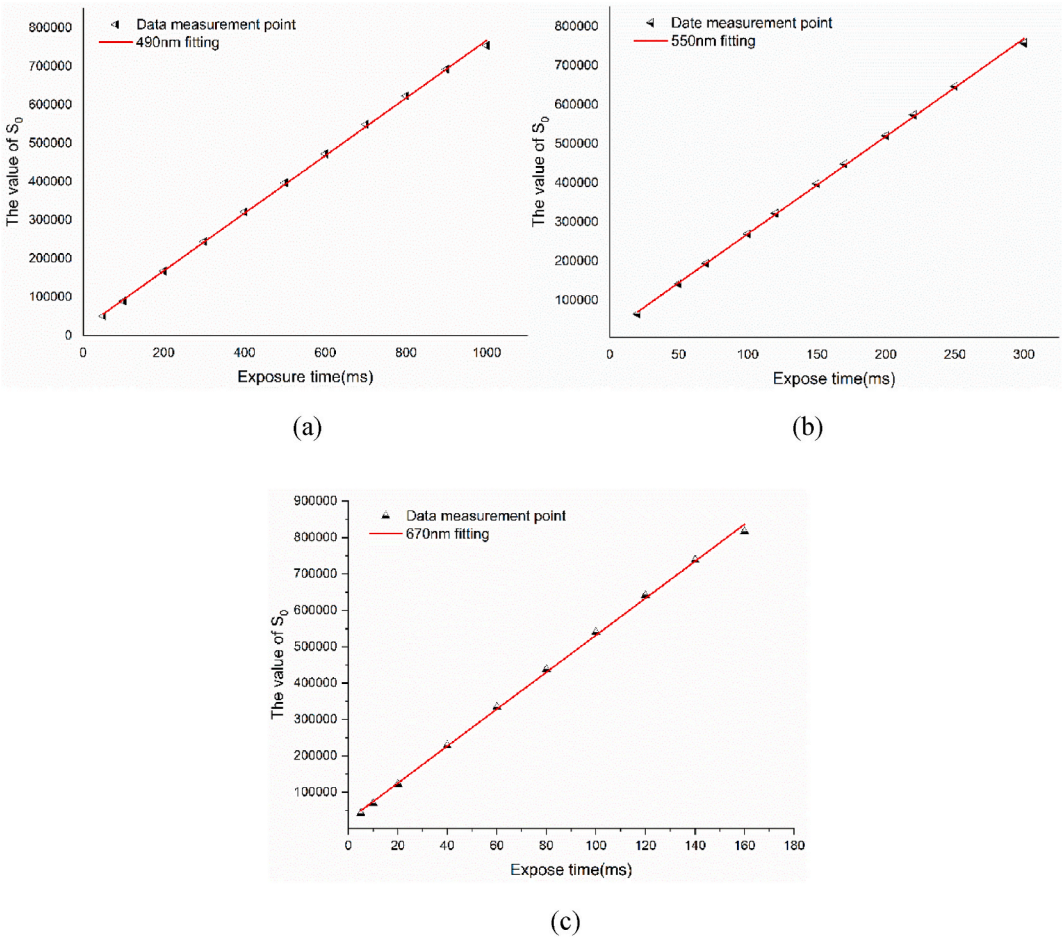

Fig. 3. (a)–(c) show the fitting results of different exposure times in 490 nm, 550 nm, and 670 nm bands, respectively.

Table 6
Model coefficients and Adjusted R-Squared values in different bands.

Wavelength (nm)	490	550	670
A	749.17658	2496.41292	5079.75129
B	18883.29446	20399.96879	23788.00203
Adj. R-Square	0.99936	0.99946	0.99886

The monochromatic radiance of the fixed integrating sphere in the 490 nm band is 0.69306 W/(cm^2·sr·nm), and the correlation between the fitting data and the real value is 0.99936 by adjusting different exposure time and using the least square method. The monochromatic radiance of the fixed integrating sphere in the 550 nm band is 1.2159 W/(cm^2·sr·nm), and the correlation between the fitting data and the real value is 0.99946. The monochromatic radiance of the fixed integrating sphere at the 670 nm band is 2.27072 W/(cm^2·sr·nm), and the correlation between the fitting data and the real value is 0.99886. Through the analysis of the above radiometric calibration data, the physical quantities of monochromatic radiance dimension corresponding to the CCD response at different exposure time and other wavelengths can also be deduced, and it can be concluded that the full polarization imager has excellent radiation stability and meets the measurement requirements.

of polarization of the transmitted light after passing through the first flat glass is expressed as follows formula (13).

$$P_1 = \left[\sin^2(i+r)\cdot\sin^2(i-r)\right] / \left[\sin^2(i+r)+\sin^2(i-r)-\sin^2(i+r)\cdot\sin^2(i-r)\right] \tag{13}$$

Where r is the refraction angle of transmitted light on the surface of flat glass, when the light from the light source passes through four pieces of flat glass with the same material and inclination angle, the polarization degree generated by the polarization state generator is shown in formula (14).

$$P = \left[(1+P_1)^4-(1-P_1)^4\right] / \left[(1+P_1)^4+(1-P_1)^4\right] \tag{14}$$

Table 7
Theoretical calculation of the degree of polarization of APOL in different bands.

Wavelength (nm)		490	550	670
Refractive index		1.52210	1.51852	1.51391
Rotation angle	0	0	0	0
	10	0.01391	0.01379	0.01364
	20	0.05756	0.05707	0.05645
	30	0.13661	0.13549	0.13405
	40	0.25911	0.25714	0.25457
	50	0.42898	0.42613	0.42243
	60	0.62861	0.62543	0.62129

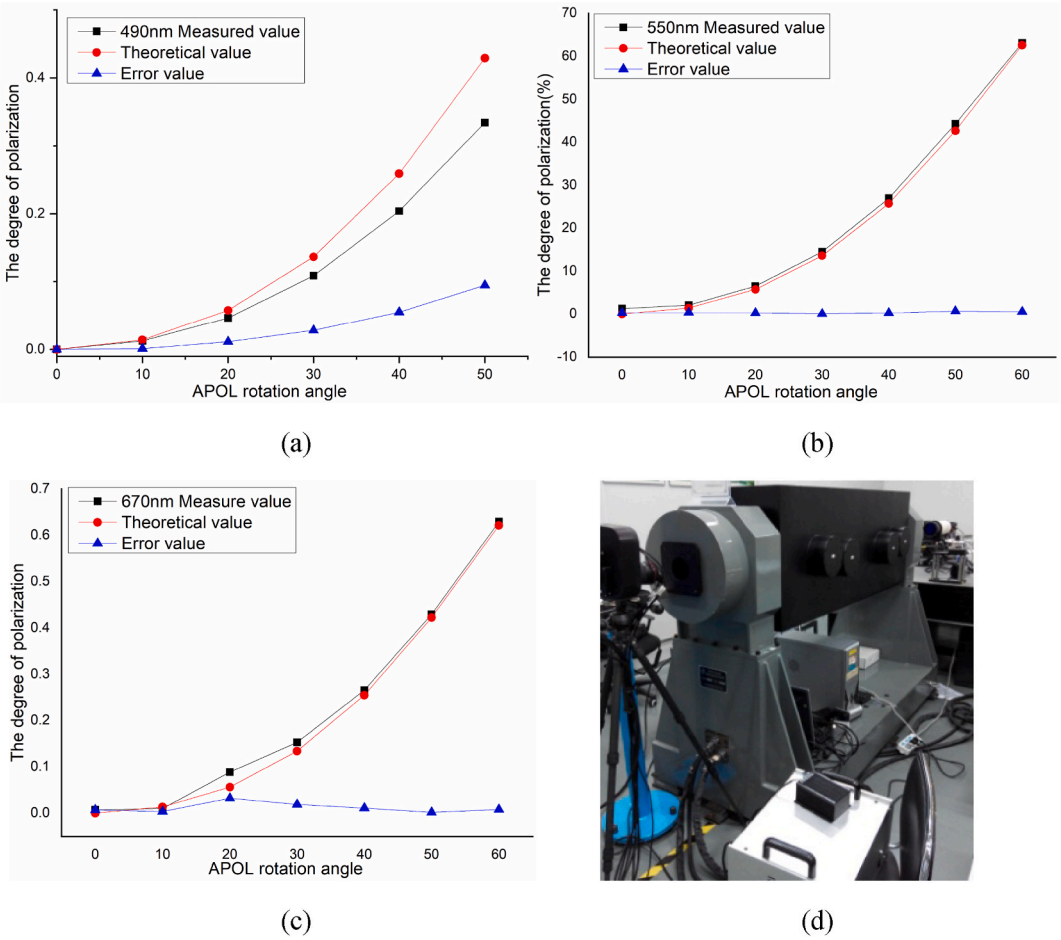

Fig. 4. (a)–(c) show the polarization calibration results at 490 nm, 550 nm, and 670 nm, respectively, and (d) shows the experimental scene.

APOL can generate polarization in the range of 0–0.72, and the difference between the theoretical value and the specific polarization light generated by APOL is less than 0.006. The experimentally measured value agrees well with the theoretical value. The refractive index is different in different wavelengths, so the polarization degree produced by adjustable polarization degree light source is different. The theoretical values calculated at different wavelengths and different glass rotation angles are shown in the following table.

According to Table 7, the refractive index of different bands is different, so the degree of polarization of polarized light emitted by APOL at the same rotation angle is different. Before polarization calibration, data preprocessing is carried out. The effect of the dark current of the polarizing camera and CCD response inconsistency caused by different installation directions of the polarizer transmission axis is deducted for correction. The polarization calibration results of the full polarization imager are shown in the following Fig. 4(a–c). The experimental scene is shown in Fig. 4(d).

The measured values for the three bands in Fig. 4(a–c) are derived from the calculation of formula (9). From the analysis of Fig. 4 (a–c), it can be seen that the polarization imager in the 490 nm band, the error has a positive correlation with the increase in the degree

of polarization light generated by APOL. Usually, in the actual observation and imaging scene of polarization remote sensing, the degree of polarization calculated by the Stokes vector is low, and the measurement accuracy is guaranteed within 2% in the area where the degree of polarization is less than 0.2. In the 550 nm band, there is a good correlation between the actual measured value and the theoretical value, so the influence of measurement deviation can be eliminated in data processing, and the polarization measurement accuracy is guaranteed within 1.5%. At the 670 nm band, the actual measured values of the polarization imager are in good agreement with APOL. Only when the rotation angle of the APOL is 20^0, the deviation is 3.23%, and the polarization calibration accuracy of other angles is less than 1%, which meets the requirements of high-precision polarimetric remote sensing detection.

4. Conclusions

Radiation stability and polarization detection accuracy are the core technical indexes of the polarization imaging instruments. To meet the needs of different application scenarios, different types of polarization detection instruments are constantly presented. Therefore, it is necessary to formulate the calibration process for polarization imaging instruments. Aiming at the calibration problem of a full polarization imager, in this paper radiometric calibration and polarization calibration are studied.

In radiometric calibration, an integrating sphere with a diameter of 2.5 m is used as the calibration light source. The response intensity analysis of the imager with the different numbers of lights on integrating sphere is carried out. Analysis and research on the radiance of the fixed integrating sphere, different exposure time, and intensity response of the imager. A mathematical model is constructed to compare and analyze the simulated data with the measured data. The results show that the correlation between simulated data and measured data in the 490 nm, 550 nm, and 670 nm bands is above 0.99 for two different radiometric calibration methods. Under the varying numbers of lights on the integrating sphere, the correlation of 490 nm data is 0.99916, 550 nm data is 0.99533, and 670 nm data is 0.99918. Under different exposure time conditions, the correlations at 490 nm, 550 nm, and 670 nm were 0.99936, 0.99946, and 0.99886, respectively. Through the analysis of radiometric calibration data, the full polarization imager has excellent radiation stability and meets the requirements of radiation measurement.

In polarization calibration, the APOL system is used as the reference polarization source. The theoretical and measured values of the degree of polarization of the 490 nm, 550 nm, and 670 nm reference light sources are analyzed, respectively. The results show that the measurement accuracy of the 490 nm band is less than 2% when the theoretical degree of polarization is less than 0.2. There is a good correlation between the actual measured value and the theoretical value in the 550 nm band, and the polarization measurement accuracy is less than 1.5%. The real calculated value in the 670 nm band agrees with APOL. Only when the APOL rotates at 20^0, the deviation is 3.23%, and the polarization calibration accuracy of other angles is less than 1%. Through the analysis of polarization calibration data, the polarization calibration accuracy of the full polarization imager is high, which meets the requirements of high-precision polarization detection. At the same time, the research in this paper provides an essential technical reference for the calibration of other polarization instruments.

Author contribution statement

Tianquan Liang: Conceived and designed the experiments; Performed the experiments; Analyzed and interpreted the data; Wrote the paper. Qingxin Tang: Analyzed and interpreted the data; Contributed reagents, materials, analysis tools or data. Quanzhou Yu: Analyzed and interpreted the data; Contributed reagents, materials, analysis tools or data.

Data availability statement

Data will be made available on request.

Declaration of competing interest

The authors declare that they have no known competing financial interests or personal relationships that could have appeared to influence the work reported in this paper.

Acknowledgments

This work was supported by the Natural Science Foundation of Shandong Province, China, grant number ZR2021MD090, ZR2023MD129, the National Natural Science Foundation of China, grant number 31800367, Discipline with Strong Characteristics of Liaocheng University-Intelligent Science and Technology under Grant 319462208.

References

[1] G.G. Stokes, On the change of refrangibility of light, Phil. Trans. Roy. Soc. Lond. 142 (1852) 463–562.
[2] J.S. Tyo, D.L. Goldstein, D.B. Chenault, et al., Review of passive imaging polarimetry for remote sensing applications, Appl. Opt. 45 (2006) 5453–5469.
[3] F. Maignan, F.M. Breon, E. Fedele, et al., Polarized reflectances of natural surfaces: spaceborne measurements and analytical modeling, Remote Sens. Environ. 113 (2009) 2642–2650.
[4] C. Chen, O. Dubovik, G.L. Schuster, et al., Multi-angular polarimetric remote sensing to pinpoint global aerosol absorption and direct radiative forcing, Nat. Commun. 13 (2022) 7459.

[5] P. Litvinov, O. Hasekamp, O. Dubovik, et al., Model for land surface reflectance treatment: physical derivation, application for bare soil and evaluation on airborne and satellite measurements, J. Quant. Spectrosc. Radiat. Transf. 113 (2012) 2023–2039.
[6] O. Dubovik, D. Fuertes, P. Litvinov, et al., A comprehensive description of multi-term LSM for applying multiple a priori constraints in problems of atmospheric remote sensing: GRASP algorithm, concept, and applications, Front. Remote Sens. 2 (2021), 706851.
[7] Z.Q. Sun, D. Wu, Y.F. Lv, Optical properties of snow surfaces: multiangular photometric and polarimetric hyperspectral measurements, IEEE Trans. Geosci. Rem. Sens. 60 (2022), 4301516.
[8] C. He, J.T. Chang, Q. Hu, et al., Complex vectorial optics through gradient index lens cascades, Nat. Commun. 10 (2019) 4264.
[9] O. Dubovik, Z.Q. Li, M.I. Mishchenko, et al., Polarimetric remote sensing of atmospheric aerosols: instruments, methodologies, results, and perspectives, J. Quant. Spectrosc. Radiat. Transf. 224 (2019) 474–511.
[10] T.Q. Liang, X.B. Sun, H. Wang, et al., Airborne polarimetric remote sensing for atmospheric correction, J. Sens. 2016 (2016), 3569272.
[11] J. Yang, T. Du, B. Niu, et al., A bionic polarization navigation sensor based on polarizing beam splitter, IEEE Access 6 (2018) 11472–11481.
[12] N.A. Rubin, G.D. Aversa, P. Chevalier, et al., Matrix fourier optics enables a compact full-Stokes polarization camera, Science 365 (6448) (2019) 1–8.
[13] N.A. Rubin, A. Zaidi, M. Juhl, et al., Polarization state generation and measurement with a single metasurface, Opt. Express 26 (17) (2018) 21455–21478.
[14] R.G.V. Holstein, J.H. Girard, J. Boer, et al., Polarimetric imaging mode of VLT/SPHERE/IRDIS II. Characterization and correction of instrumental polarization effects, Astron. Astrophys. 633 (2020) A64.
[15] P.Y. Deschamps, F.M. Breon, M. Leroy, et al., The POLDER mission: instrument characteristics and scientific objectioves, IEEE Trans. Geosci. Rem. Sens. 32 (1994) 598–615.
[16] J. Chowdhary, B. Cairns, F. Waquet, et al., Sensitivity of multiangle, multispectral polarimetric remote sensing over open oceans to water-leaving radiance: analyses of RSP data acquired during the MILAGRO campaign, Remote Sens. Environ. 118 (2012) 284–308.
[17] T.Q. Liang, X.J. Duan, Q.X. Tang, et al., Research of dental caries lesion based on the visible-near infrared spectrum polarization detection, Spectrosc.Spect. Anal. 41 (1) (2021) 145–149.
[18] Z.Q. Li, W.Z. Hou, J. Hong, et al., The polarization crossfire (PCF) sensor suite focusing on satellite remote sensing of fine particulate matter PM2.5 from space, J. Quant. Spectrosc. Radiat. Transf. 286 (2022), 108217.
[19] B. Fougnie, T. Marbach, A. Lacan, et al., The multi-viewing multi-channel multi-polarisation imager- overview of the 3MI polarimetric mission for aerosol and cloud characterization, J. Quant. Spectrosc. Radiat. Transf. 219 (2018) 23–32.
[20] X.B. Li, F. Goudail, S.C. Chen, Self-calibration for Mueller polarimeters based on DoFP polarization imagers, Opt. Lett. 47 (6) (2022) 1415–1418.
[21] G.V. Harten, D.J. Diner, B.J.S. Daugherty, et al., Calibration and validation of airborne multiangle SpectroPolarimetric imager (AirMSPI) polarization measurements, Appl. Opt. 57 (16) (2018) 4499–4513.
[22] H.F. Wang, P. Zhang, D.K. Yin, et al., Shortwave infrared Multi-Angle Polarization Imager (MAPI) onboard Fengyun-3 precipitation Satellite for enhanced cloud characterization, Rem. Sens. 14 (2022) 4855.
[23] J.S. Baba, J.R. Chung, A.H. Delaughter, et al., Development and calibration of an automated Mueller matrix polarization imaging system, J. Biomed. Opt. 7 (3) (2002) 341–349.
[24] J.J. Shi, M.F. Li, Y.D. Hu, et al., Laboratory calibration of an ultraviolet–visible imaging Spectropolarimeter, Rem. Sens. 14 (2022) 3898.
[25] E. Compain, S. Poirier, B. Drevillon, General and self-consistent method for the calibration of polarization modulators, polarimeters, and Mueller-matrix ellipsometers, Appl. Opt. 38 (16) (1999) 3490–3502.
[26] T.Q. Liang, Q.X. Tang, Q.Z. Yu, et al., Measurement of polarization-sensitive characteristic of scientific CCD detector, Optik 223 (2020), 165593.
[27] C. Lane, D. Rode, T. Rosgen, Calibration of a polarization image sensor and investigation of influencing factors, Appl. Opt. 61 (6) (2022) C37–C45.
[28] S.B. Powell, V. Gruev, Calibration methods for division-of-focal-plane polarimeters, Opt. Express 21 (18) (2013) 21039–21055.